Colloidal Quantum Dots as Probes of Excitation Field Enhancement in Photonic Antennas

Heykel Aouani,[†] Stella Itzhakov,[‡] David Gachet,[†] Eloïse Devaux,[§] Thomas W. Ebbesen,[§] Hervé Rigneault,[†] Dan Oron,[‡] and Jérôme Wenger[†,*]

[†]Institut Fresnel, Aix-Marseille Université, CNRS, Ecole Centrale Marseille, Campus de St Jérôme, 13397 Marseille, France, [‡]Department of Physics of Complex Systems, Weizmann Institute of Science, Rehovot 76100, Israel, and [§]Institut de Science et d'Ingénierie Supramoléculaires, Université de Strasbourg, CNRS, 8 allée G. Monge, 67000 Strasbourg, France

ABSTRACT Optical antennas are essential devices to interface light to nanoscale volumes and locally enhance the electromagnetic intensity. Various experimental methods can be used to quantify the antenna amplification on the emission process, yet characterizing the antenna amplification at the excitation frequency solely is a challenging task. Such experimental characterization is highly needed to fully understand and optimize the antenna response. Here, we describe a novel experimental tool to directly measure the antenna amplification on the excitation field independently of the emission process. We monitor the transient emission dynamics of colloidal quantum dots and show that the ratio of doubly to singly excited state photoluminescence decay amplitudes is an accurate tool to quantify the local excitation intensity amplification. This effect is demonstrated on optical antennas made of polystyrene microspheres and gold nanoapertures, and supported by numerical computations. The increased doubly excited state formation on nanoantennas realizes a new demonstration of enhanced light-matter interaction at the nanoscale.

KEYWORDS: colloidal quantum dots · plasmonics · nanoantennas · microspheres · metal nanoapertures · fluorescence enhancement · Auger recombination

Optical antennas are essential devices to interface light to nanoscale elements and focus electromagnetic energy to subwavelength dimensions much beyond the classical diffraction limit.[1] To meet this goal, most optical antennas take advantage of surface plasmon modes on metal nanostructures to squeeze light into nanoscale volumes.[2] Recent advances in plasmonics open new routes to generate, manipulate, and detect light at the nanoscale, with applications in near-field microscopy,[2] enhanced light-matter interactions,[3,4] surface-enhanced molecular sensing,[5,6] or photovoltaics.[7]

In that context, a thorough understanding of the optical response of antennas is essential.[8] One of the most important characteristics of an optical antenna lies in its ability to locally enhance the electromagnetic intensity. Estimates of the electromagnetic enhancement are generally deduced from measurements of the optical emission phenomenon to amplify fluorescence,[5,6] Raman scattering,[9] or nonlinear photoluminescence.[3,10] These measurements provide an accurate quantification of the *global* gain brought by the antenna during both excitation and emission processes. However, extracting the contribution of the antenna at the *excitation* wavelength only is a challenging task, as the detected luminescence signal results from an intricate combination of modifications on excitation intensity, emission rate, and collection efficiency.[6,11]

Experimental characterization of the antenna amplification for the excitation process only is a crucial task to provide the designer with direct feedback on the antenna properties. Such characterization is highly needed to understand the nontrivial downscaling relationship between radiowave and optical regimes,[1] and to optimize the electromagnetic amplification for the various applications.[2] A novel experimental approach based on a modified dark-field scattering setup has been recently reported.[8] This provides useful information on various relevant parameters such as antenna resonant frequencies, bandwidths, and radiation patterns. However, estimates on local excitation intensity enhancement turn out to be difficult based on the complex detection geometry. Another approach to determine the antenna amplification for the excitation process relies on a procedure based on fluorescent molecules to probe the local field enhancement.[11] Combining fluorescence correlation spectroscopy (FCS) and fluorescence lifetime measurements, the respective contributions of excitation and emission gains can be quantified from the

*Address correspondence to jerome.wenger@Fresnel.fr.

Received for review April 16, 2010 and accepted July 13, 2010.

Published online July 21, 2010. 10.1021/nn1009209

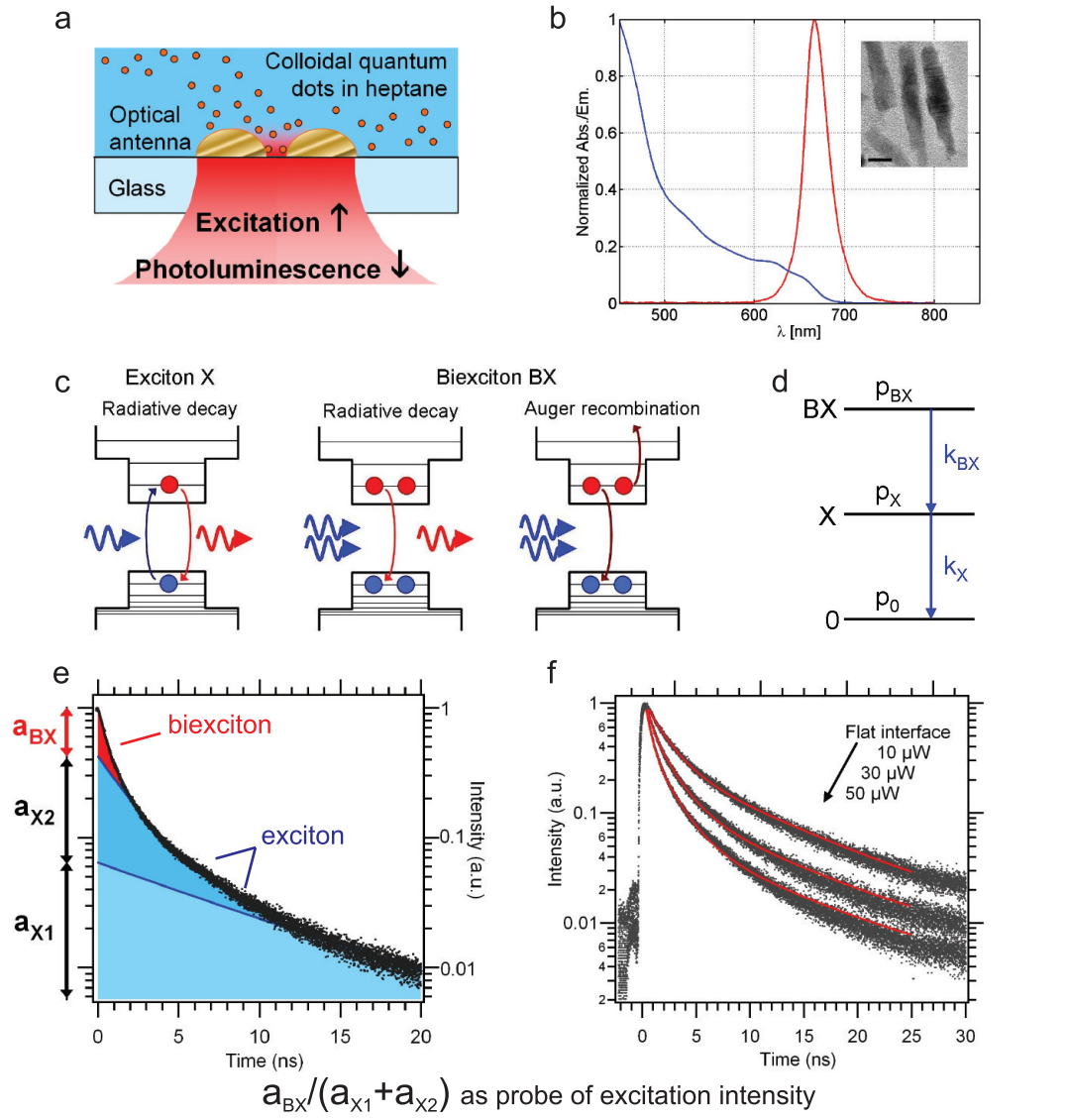

Figure 1. (a) Configuration to analyze a generic antenna made of a gold nanoparticle dimer. (b) Normalized absorption (blue) and emission (red) spectra of the CdSe/CdS/ZnS QD sample. The emission, centered at 670 nm, has a full-width at half-maximum of 31 nm. The inset depicts a TEM image of several QDs. Scale bar is 10 nm. (c) Schematic description of the decay routes for singly (exciton X) and doubly excited (biexciton BX) states. (d) Representation of the kinetic model used in the text. (e) Photoluminescence decay curves and contributions of X and BX population decay amplitudes for a flat glass interface at 50 μW average excitation power. (f) Photoluminescence decay curves for a flat glass interface at increasing excitation powers showing a growing contribution of the BX population.

overall fluorescence enhancement. A third approach takes advantage of the broad absorption spectrum of colloidal quantum dots to probe the photoluminescence intensity on and off the antenna resonance.[12] However, these techniques require an extensive series of measurements and do not provide direct access to the excitation gain in a single measurement.

In this contribution, we describe a novel and direct approach to quantify the electromagnetic amplification on an optical antenna for the excitation process only. It relies on sequential resonant photon absorption in colloidal quantum dots (QDs). Unlike molecular systems, QDs can sustain multiple excited states.[13,14] In this contribution, we focus on the contributions of singly (exciton X) and doubly (biexciton BX) excited states,[15−18] and show that the ratio of the BX to the X state photoluminescent decay amplitudes provides a direct measure of the local excitation intensity. This can thus be used as a powerful tool for characterizing optical antenna responses on the excitation process independently of the emission process. Moreover, in a single measurement, the single exciton lifetime and intensity can be measured, from which the fluorescence and emission gains can also be deduced. A schematic description of the system is depicted in Figure 1a.

We demonstrate this principle with core/shell/shell CdSe/CdS/ZnS QDs, whose properties are shown in Figure 1b. The QDs are rodlike, having a peak emission at 670 nm (corresponding to a diameter of nearly 10 nm, as shown in the inset TEM image) and typical aspect

ratio of 5. The photon absorption mostly occurs at the thicker part of the rod, where the CdSe core is embedded. We point out that the data presented here are averages over several QDs that surround the optical antenna. Therefore, the excitation intensity enhancement has to be understood as a spatially averaged enhancement over the analysis volume. Most importantly for the current application, the QDs exhibit both a high (>50%) quantum yield and a relatively long biexciton Auger recombination lifetime of about 500 ps. Further information can be found in the synthesis section as well as in the Supporting Information.

We use the QDs to probe the local excitation intensity amplification on optical antennas made of dielectric microspheres and metal nanoapertures under focused illumination. Dielectric microspheres realize one of the simplest forms of optical antenna to overcome the diffraction limits and enhance the fluorescence detection.[19] Their dielectric nature ensures that no quenching losses affect the QDs lifetime measurements. To reach higher gains in excitation intensity, we take advantage of plasmonic resonances on gold nanoapertures. Metal nanoapertures form reliable test antennas, as they can be reproducibly fabricated, and have been demonstrated to be sensitive platforms for enhanced fluorescence detection.[20,21]

RESULTS AND DISCUSSION

BX/X Ratio as a Probe of Local Excitation Intensity. Figure 1 briefly summarizes the concepts involved. As a consequence of the strong quantum confinement of the free charge carriers, the lifetimes of the multiply excited states strongly depend on the number of generated charge carriers.[14] As depicted in Figure 1c, the decay from a BX to a X state can take two routes: either radiative with emission of one photon or nonradiative through Auger recombination. The Auger lifetime typically scales with the QD's volume (and also exhibits some shape dependence) and usually ranges between ten and a few hundreds of picoseconds, whereas the X state radiative lifetime can approach tens of nanoseconds. The respective amplitudes of the X and BX state decays can therefore be addressed by monitoring the QD's transient emission dynamics.[15,16] Hereafter, we consider that both the excitation pulse duration and the instrument temporal resolution are much shorter than the faster multiexciton dynamic (namely Auger recombination), so that the contributions of BX and X states to the photoluminescence decay can be unambiguously measured.

Below photoluminescence saturation, the X state mostly results from the absorption of a *single* photon while the BX state is created after the sequential absorption of *two* photons. Immediately after pulsed photoexcitation, the X and BX relative populations thus scale linearly and quadratically (respectively) with the excitation intensity. BX state formation can thus be seen as a second-order nonlinear optical process.[18] Decay from the BX state can take two routes: either radiative with emission of one photon or nonradiative recombination through Auger relaxation.[14] However, it is important to note that the BX state relaxes to the X state regardless of the nature of the relaxation process, and that at most one *single* photon is emitted during the BX to X collapse.

In the following we demonstrate that the ratio of doubly to singly excited state photoluminescence decay amplitudes is proportional to the local excitation intensity and is not dependent on the emission rate. We represent the multiexciton relaxation under pulsed excitation by using a first-order kinetic model. We restrict the discussion to the case when only the singly excited state (exciton X) and doubly excited state (biexciton BX) contribute to the detected QD photoluminescence signal. A more general discussion can be found for instance in the Supporting Information of ref 17. Figure 1(d) illustrates the kinetic model and notations. $p_i(t)$ are the relative populations of the *i*-excitonic state, k_i are the *total* decay rates. After pulsed excitation, the populations evolve as

$$\begin{aligned} p_{BX}(t) &= p_{BX}^0 e^{-k_{BX}t} \\ p_X(t) &= \left(p_X^0 + \frac{k_{BX}}{k_{BX} - k_X} p_{BX}^0\right) e^{-k_X t} - \frac{k_{BX}}{k_{BX} - k_X} p_{BX}^0 e^{-k_{BX}t} \end{aligned} \quad (1)$$

Here p_i^0 denote the *initial* relative populations, taken just after excitation. As the biexciton decay rate k_{BX} is dominated by the Auger recombination rate, $k_{BX} \gg k_X$, and $k_{BX}/(k_{BX} - k_X) \approx 1$. The populations can thus be simplified as

$$\begin{aligned} p_{BX}(t) &= p_{BX}^0 e^{-k_{BX}t} \\ p_X(t) &= (p_X^0 + p_{BX}^0) e^{-k_X t} - p_{BX}^0 e^{-k_{BX}t} \end{aligned} \quad (2)$$

The second term in $e^{-k_{BX}t}$ in the p_X population relates to the fact that the X population actually grows as the BX population decays.

We are primarily interested in the photoluminescence signal $s(t)$ that is detected in the TCSPC experiment. The measured photoluminescence relates to the multiexcitonic populations as

$$s(t) = k_X^{rad} p_X(t) + k_{BX}^{rad} p_{BX}(t) = a_X e^{-k_X t} + a_{BX} e^{-k_{BX}t} \quad (3)$$

where k_i^{rad} is the *radiative* decay rate for the *i*th mulitexciton state; a_X and a_{BX} are the amplitudes of the transient components in the photoluminescence signal $s(t)$ of characteristic decay times $\tau_X = 1/k_X$ and $\tau_{BX} = 1/k_{BX}$, respectively. The amplitudes a_X and a_{BX} are measured by the time-correlated single-photon counting (TCSPC) experiment. Substituting eq 2 into eq 3 gives the following expressions for the X and BX amplitudes:

$$a_X = k_X^{rad}(p_X^0 + p_{BX}^0)$$
$$a_{BX} = (k_{BX}^{rad} - k_X^{rad})p_{BX}^0 \quad (4)$$

Since all multiexcitonic states eventually collapse into an X state, both BX and X initial populations contribute to the X photoluminescence signal. The a_X amplitude is therefore proportional to the X radiative rate and to the *total* population $p_{Tot}^0 = p_X^0 + p_{BX}^0$ that starts in an excited state (X or higher). The a_{BX} amplitude is proportional to the difference in X and BX radiative rates, as a consequence of the $e^{-k_{BX}t}$ temporal dependence of the X population p_X. The X and BX radiative decay rates are different, and the latter is difficult to infer experimentally due to the strong Auger recombination process. However, it is known that the X and BX states are nearly degenerate in energy.[15,16] It has also been previously shown that k_{BX}^{rad} typically exceeds k_X^{rad} by a factor $r \approx 2-3$, that is mostly fixed by the degeneracy of the BX state.[18,22] The X and BX amplitudes thus rewrite

$$a_X = k_X^{rad} p_{Tot}^0$$
$$a_{BX} = k_X^{rad}(r-1)p_{BX}^0 \quad (5)$$

The above equations already demonstrate that *both* a_X and a_{BX} are proportional to the *same* radiative rate k_X^{rad}.

We now turn to express the initial populations p_X^0 and p_{BX}^0. When QDs are excited above their band edge, photon absorption events can be considered as independent and are described by a Poissonian statistics following[22]

$$P(k,\bar{n}) = \bar{n}^k \frac{e^{-\bar{n}}}{k!} \quad (6)$$

where $\bar{n}$ and k are the average and absorbed number of excitation photons per QD per pulse, respectively. The total (X and BX states) initial population p_{Tot}^0 is proportional to the probability of getting at least one photon absorbed,

$$p_{Tot}^0 \propto 1 - P(0,\bar{n}) = 1 - e^{-\bar{n}} \quad (7)$$

while the initial BX population p_{BX}^0 is proportional to the probability of getting over one photon absorbed,

$$p_{BX}^0 \propto 1 - P(0,\bar{n}) - P(1,\bar{n}) = 1 - (1+\bar{n})e^{-\bar{n}} \quad (8)$$

which finally gives the following expressions for the X and BX amplitudes:

$$a_X \propto k_X^{rad}(1 - e^{-\bar{n}})$$
$$a_{BX} \propto k_X^{rad}(r-1)(1 - (1+\bar{n})e^{-\bar{n}}) \quad (9)$$

The most important point of this demonstration is that *both* a_X and a_{BX} are proportional to the *same* radiative rate k_X^{rad}. Dealing with photonic antennas to enhance the total photoluminescence signal, both a_X and a_{BX} undergo the *same* emission rate enhancement. While computing the ratio of the BX to the X state photoluminescent decay amplitudes, the emission rate contribution cancels out, and only a term proportional to the local excitation intensity remains:

$$\frac{a_{BX}}{a_X} = (r-1)\frac{1 - (1+\bar{n})e^{-\bar{n}}}{1 - e^{-\bar{n}}} \quad (10)$$

As $r - 1 \approx 1$ is a constant, the a_{BX}/a_X ratio only depends on the average number of absorbed photons $\bar{n}$, which is a direct probe of the local excitation intensity. For excitations below saturation $\bar{n} \ll 1$, $a_X \propto \bar{n}$ and $a_{BX} \propto \bar{n}^2$, hence a_{BX}/a_X scales *linearly* as the excitation intensity. Hereafter, we will refer to a_{BX}/a_X as the "BX/X ratio". This BX/X ratio thus provides a direct access to the local excitation intensity, and can be used to characterize optical antennas. An increase in this ratio on a nanoantenna as compared to a flat interface (for the same average excitation power) is a direct demonstration of an increased local excitation intensity.

Calibration on a Flat Glass Interface. We start the experimental study by calibrating the QDs transient emission dynamics on a flat glass interface. This will serve as a reference for the next investigations on optical antennas. Figure 1e and Figure 1f display TCSPC histograms recorded for increasing laser powers on QDs dispersed on a flat glass-heptane interface. At low excitation powers, two components (with amplitudes a_{X_1} and a_{X_2}, proportional to the initial X state population)[17] are already visible in the decay curves. This dual-exponential decay may originate from a statistical mixture of two QDs populations, from charging or from temporal fluctuations in the exciton lifetime.[23] As the excitation power is increased, a significant fast transient component arises. Its amplitude a_{BX} is proportional to the initial BX state population.[17]

The TCSPC data is modeled using the following expression:

$$s(t) = (a_{X_1}e^{-t/\tau_{X_1}} + a_{X_2}e^{-t/\tau_{X_2}}) + a_{BX}e^{-t/\tau_{BX}} \quad (11)$$

In the analysis, the lifetimes are fixed to $\tau_{X_1} = 9.5$ ns, $\tau_{X_2} = 2.0$ ns, and $\tau_{BX} = 0.5$ ns. The a_{X_1}, a_{X_2} exciton, and a_{BX} biexciton decay amplitudes are left as the only free parameters. We found that a_{X_1} and a_{X_2} increase linearly with the excitation power, while a_{BX} increases quadratically. As demonstrated above, the ratio $a_{BX}/(a_{X_1} + a_{X_2})$ (referred as "BX/X ratio" in the following) depends only on the average number of absorbed photons and is a direct probe of the local excitation intensity. This is evidenced by the linear behavior of the BX/X ratio while increasing the excitation power as shown in Figure 2 and Figure 3.

Excitation Field Enhancement on Dielectric Microspheres. We now use the BX/X ratio to probe the local *excitation* intensity enhancement on a simple optical antenna made of a polystyrene microsphere. When a microsphere is illuminated with a tightly focused Gaussian beam, it was shown to overfocus light in a region with subwave-

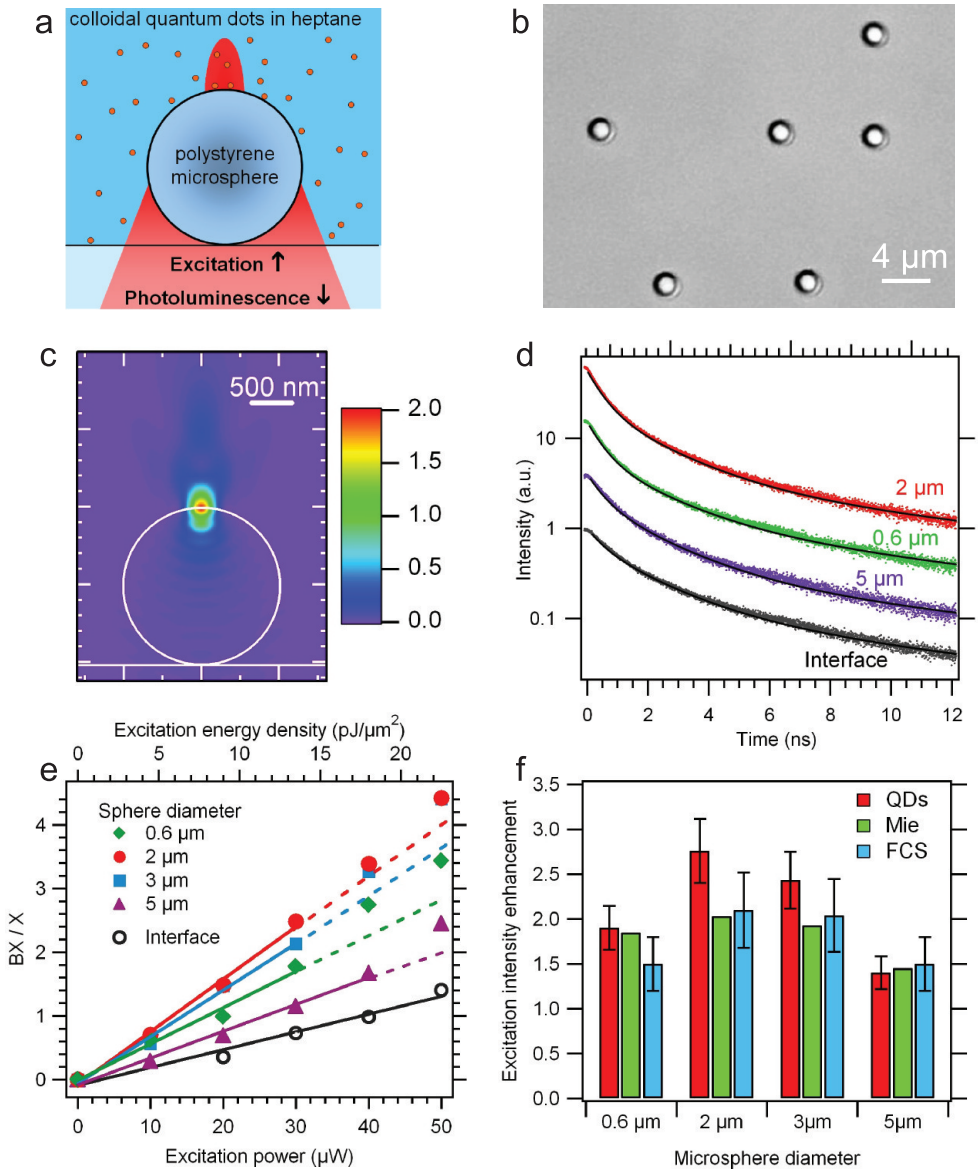

Figure 2. (a) Experimental configuration schematics with a single microsphere. (b) Optical microscope image of 2 μm diameter polystyrene microspheres fixed to a glass slide. (c) Field intensity distribution near a polystyrene microsphere (diameter, 2 μm; refractive index, 1.59) illuminated by a focused Gaussian beam at λ = 633 nm with 1.2 numerical aperture. The outer medium refractive index is set to 1.33, the glass slide refractive index is 1.5. (d) Photoluminescence decay curves on polystyrene microspheres at 30 μW average excitation power (curves shifted for clarity). (e) BX/X ratio *versus* excitation power for microspheres and flat glass interface. The increase in the slope for microspheres yield the local excitation intensity enhancement. Only the data with BX/X < 2 are considered for the determination of the slope. (f) Excitation enhancements determined from the BX/X slopes and comparison to other methods: numerical simulations using Mie theory and FCS measurements.

length dimensions in both the transverse and longitudinal directions, creating high local intensities (see Figure 2a−c).[24,25] This effect stems from interferences between the field scattered by the sphere and the high angular components of the incident Gaussian beam passing aside the sphere. Microspheres therefore constitute efficient and cost-effective devices to enhance the fluorescence emission up to five times, without requiring expensive nanofabrication facilities.[26]

Figure 2d shows photoluminescence decay curves for different microsphere diameters at a fixed excitation power. The fast (BX) transient component is clearly larger on the microsphere than for the flat interface. We point out that the X and BX lifetimes are unaffected by the microsphere as compared to the case of the flat interface as a consequence of the dielectric nature of the sphere. Therefore, in the TCSPC data analysis based on eq 11, we keep the same values for τ_j for both the microsphere and the flat interface.

Figure 2e displays the BX/X ratios deduced from numerical fits of the TCSPC data for increasing excitation powers. As long as BX/X < 2 (average powers below 30 μW or energy densities below 14 pJ/μm^2), the BX/X ratios follows a linear relationship with the excitation power. Under these conditions, the contributions of higher excited states and saturation effects are still

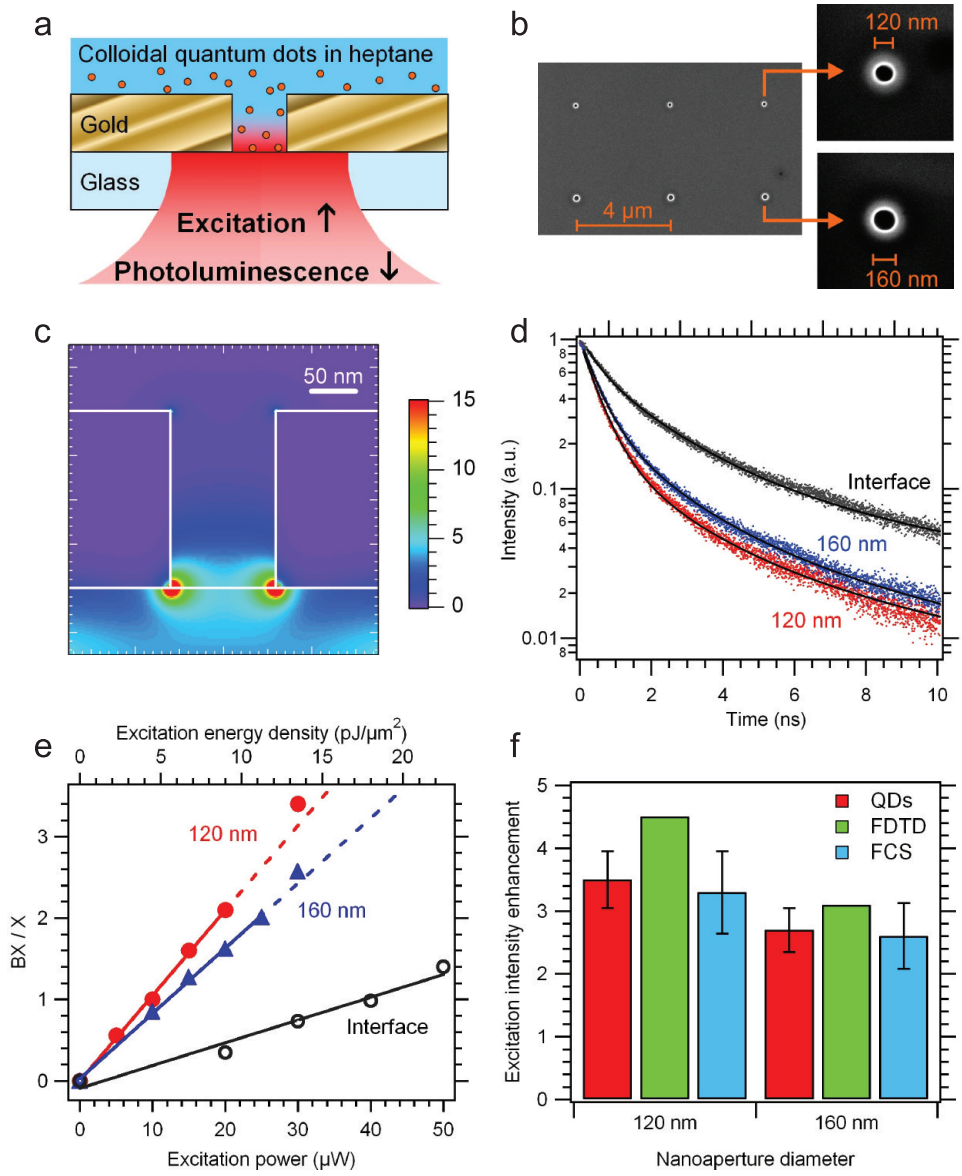

Figure 3. (a) Experimental configuration schematics with a single nanoaperture. (b) Electron microscope images of 120 and 160 nm apertures milled in gold. (c) Field intensity distribution on a gold nanoaperture (diameter 120 nm) illuminated at λ = 633 nm. The inner medium refractive index is set to 1.33, the glass slide refractive index is 1.5. (d) Photoluminescence decay curves on gold nanoapertures at 30 μW average excitation power. (e) BX/X ratio versus excitation power for gold nanoapertures and flat glass interface. Only the data with BX/X< 2 are considered to determine the slope. (f) Excitation enhancements determined from the BX/X ratios and comparison to other methods: FDTD numerical simulations and FCS measurements.

relatively small. For higher excitation powers, the BX/X exceeds the linear trend and grows more quickly due to higher multiple excited state contribution, and faster saturation of X states relative to the BX.[18]

The increase in the slope of the curves in Figure 2e (as compared to the reference case of the flat interface) is directly related to the excitation intensity amplification brought by the optical antenna. For instance, for a 2 μm sphere, we find a BX/X slope of 0.078 μW^{-1}, while for the flat interface we have 0.028 μW^{-1}. The excitation intensity enhancement in that case is thus 0.078/0.028 = 2.78. Unity excitation intensity enhancement is to be understood as compared to focusing on a flat glass interface.

Figure 2f summarizes the excitation intensity enhancement factors deduced from (i) BX/X ratios on colloidal QDs, (ii) numerical simulations based on Mie theory,[25] and (iii) FCS-based procedure on organic dyes.[26] Good correspondence is demonstrated between the different methods, showing that a 2-fold increase in excitation intensity beyond the diffraction limit can be reached elegantly using microspheres of 2 μm diameter.

Excitation Field Enhancement on Gold Nanoapertures. To reach higher gains in excitation intensity, we take advantage of plasmonic resonances on nanoapertures milled in optically thick gold films (see Figure 3a−c). Similar metal nanoapertures have been demonstrated

as platforms for enhanced single molecule fluorescence detection with gains up to 25×.[11,21] Despite our QDs relatively large shape, we did not observe any effect of their size preventing their diffusion into the nanoapertures. We tested several apertures of the same diameter and measured an experimental deviation of less than 10%, which mostly results from minor nanofabrication deficiencies.

Figure 3d compares typical photoluminescence decay curves for 120 and 160 nm diameter gold apertures and flat glass interface for the same excitation power. As for microspheres, the fast (BX) transient component is again enhanced while working with nanoapertures. In the latter case, the X lifetimes are reduced to $\tau_{X_1} = 6.4$ ns and $\tau_{X_2} = 1.65$ ns, as a consequence of metal quenching. The BX lifetime $\tau_{BX} = 0.5$ ns is dominated by the Auger recombination process and is therefore not noticeably affected by the metal aperture. Lifetime quenching by the aperture is shown hereafter to have no impact on the practical implementation of our method, which is valid as long as the X and BX lifetimes can be resolved by the TCSPC system.

Figure 3e displays the BX/X ratios for increasing excitation powers. BX/X ratios have a linear relationship with the excitation power for average powers below 25 μW (energy densities below 12 pJ/μm^2). The increase of the slope as compared to the flat interface case is used to quantify the excitation intensity enhancement.

Figure 3f summarizes the excitation intensity enhancement factors found for nanoapertures from (i) BX/X ratios on colloidal QDs, (ii) FDTD-based numerical simulations,[27] and (iii) FCS-based procedure on organic dyes.[11] Satisfactory correspondence is also demonstrated in that case between the different methods. We point out that nanofabrication challenges and spatial inhomogeneities in the electromagnetic distribution inside the nanoaperture make it difficult to experimentally reach the enhancements predicted from theory.

CONCLUSIONS

Various spectroscopic methods (fluorescence, Raman scattering, photoluminescence) can be used to quantify the *overall* amplification brought by an optical antenna on the emitted signal. However, extracting the contribution of the excitation intensity enhancement is a challenging task. Here, we provide the optical antenna designer with a novel experimental tool to directly characterize the antenna amplification on the excitation field independently on the emission process. Monitoring the transient emission dynamics of colloidal quantum dots, we show that the ratio BX/X of doubly to singly excited state photoluminescence decay amplitudes can be used as an accurate tool to quantify the local excitation intensity increase on optical antennas made of polystyrene microspheres or gold nanoapertures. A single photoluminescence decay measurement is enough, hereby providing a direct and efficient tool to characterize optical antennas at the excitation wavelength solely. As BX formation is a doubly resonant process, the required pulse energies are orders of magnitude lower than that for other second-order nonlinear processes. Moreover, as the BX lifetime is typically in the hundreds of picoseconds, there is no need for ultrashort laser pulses with duration below ten picoseconds. This further reduces the requirements for pulse peak powers. We thus believe that our method holds great potential for direct antenna characterization at the excitation frequency. Altogether, the increase in biexciton state formation on nanoantennas depicts a new form of enhanced light-matter interaction at the nanoscale.

METHODS

Synthesis of CdSe/CdS/ZnS QDs. A mixture of cadmium oxide (CdO), *n*-tetradecylphosphonic acid (TDPA), and 1-octadecene (ODE) was heated under argon to 280 °C in a three-neck flask. Following, the stock solution of trioctylphosphine selenium (TOPSe) was quickly injected to the hot solution. The growth temperature was then reduced to 250 °C until the dots reached the desired diameter. The CdS and ZnS shells were synthesized using a dropwise injection of 1:1 molar ratio Cd/S and Zn/S solutions, respectively. This results in elongated rodlike QDs, with a typical aspect ratio of 5, thicker at their center and thinning toward the edges. The QDs diluted in heptane exhibit a band edge emission centered at 670 nm and are excited at 636 nm. They exhibit a quantum yield of over 50% (measured *vs* an organic dye solution), which is high for CdSe QDs emitting at this wavelength. Further details of the synthesis and characterization are given in the Supporting Information.

Experimental Setup. Our experimental setup is based on a confocal inverted microscope with a NA = 1.2 water-immersion objective. The excitation source is provided by a picosecond laser diode operating at 636 nm (PicoQuant LDH-P-635), with pulse duration of 50 ps, and repetition rate set to 20 MHz. The laser profile is spatially filtered by a single mode fiber to provide diffraction-limited focusing by the microscope objective (calibrated waist of 260 nm). The laser polarization is set to linear.

The backward-emitted fluorescence is collected *via* the microscope objective, and filtered from the scattered laser light by a dichroic mirror (Omega Filters 650DRLP) and a long-pass filter (Omega Filters 640AELP). A 30 μm confocal pinhole conjugated to the microscope objective focal plane rejects out-of-focus light.

Single photon detection is performed by fast avalanche photodiodes (PicoQuant Micro-Photon-Device MPD-5CTC) with 670 ± 20 nm fluorescence bandpass filters. Appropriate neutral density filters in front of the APDs ensure that the detected count rates do not exceed 2% of the repetition rate (400 000 detected events per second) to avoid photon pile-up artifacts. Lastly, transient emission dynamics are analyzed by a fast time-correlated single photon counting module (PicoQuant PicoHarp 300). The overall temporal resolution of our setup is measured to 120 ps.

Microspheres and Nanoapertures Preparations. Polystyrene microspheres of calibrated diameter (Fluka Chemie GmbH, $d_s = 1$, 1.5, 2, or 3 μm; dispersion, <0.1%; refractive index, 1.59) were diluted in pure water and dispersed on a cleaned microscope glass coverslip to reach isolated spheres per 10 × 10 μm^2. Air drying of water solvent ensures microspheres adhesion to the substrate even if subsequent solvent is added afterward.

Nanoapertures were milled by focused ion beam (FEI Strata DB235) on 200 nm thick gold films deposited using reactive DC magnetron sputtering. Adhesion between the gold film and the glass coverslip substrate is ensured by a layer of 10 nm chromium oxide Cr_2O_3.

Numerical Simulations. Three-dimensional numerical simulations of the field distribution near a microsphere are performed using Lorentz−Mie theory.[25,26] The incident linearly polarized Gaussian beam is simulated using first-order Davis coefficients with the beam shape parameter corresponding to the experimental configuration of NA = 1.2. The numerical integration of the field intensity is made over the upper surface of the sphere.

Numerical modeling on nanoapertures is based on the finite-difference time-domain FDTD method using Rsoft Fullwave version 6.0. The model considers a computational space of 0.4 × 0.4 × 0.4 μm^3, with perfectly matched layers boundary conditions on all faces. A glass substrate is put underneath a 200 nm thick layer of gold, the upper region and the inner of the aperture being water. Gold dielectric properties are incorporated as measured by spectroscopic ellipsometry.[28] Excitation at 636 nm is launched incoming from the glass side. Electromagnetic intensity is measured and averaged over the plane 5 nm inside the aperture, not taking into account the 5 nm region close to the metal edges. Comparison to other methods using finite elements[29] or differential theory[30] ensure relevance of the results.

Acknowledgment. The authors acknowledge stimulating discussions with N. Bonod, A. Devilez, B. Stout, E. Popov, D. Gérard, and S. Blair. This research has been conducted in the scope of the CNRS-Weizmann NaBi European associated laboratory. This research was partly funded by the French Agence Nationale de la Recherche under contract ANR-07-NANO-006-03 "ANTARES", and by the European Research Council under contract 227577 "Plasmonics.

Supporting Information Available: Detailed description of the CdSe/CdS/ZnS QD synthesis. This material is available free of charge *via* the Internet at http://pubs.acs.org.

REFERENCES AND NOTES

1. Bharadwaj, P.; Deutsch, B.; Novotny, L. Optical Antennas. *Adv. Opt. Photonics* **2009**, *1*, 438–483.
2. Schuller, J. A.; Barnard, E. S.; Cai, W. S.; Jun, Y. C.; White, J. S.; Brongersma, M. L. Plasmonics for Extreme Light Concentration and Manipulation. *Nat. Mater.* **2010**, *9*, 193–204.
3. Muhlschlegel, P.; Eisler, H. J.; Martin, O. J. F.; Hecht, B.; Pohl, D. W. Resonant Optical Antennas. *Science* **2005**, *308*, 1607–1609.
4. Kim, S.; Jin, J.; Kim, Y.-J.; Park, I.-Y.; Kim, Y.; Kim, S.-W. High-Harmonic Generation by Resonant Plasmon Field Enhancement. *Nature* **2008**, *453*, 757–760.
5. Fu, Y.; Lakowicz, J. R. Modification of Single Molecule Fluorescence near Metallic Nanostructures. *Laser & Photon. Rev.* **2009**, *3*, 221–232.
6. Kinkhabwala, A.; Yu, Z. F.; Fan, S. H.; Avlasevich, Y.; Mullen, K.; Moerner, W. E. Large Single-Molecule Fluorescence Enhancements Produced by a Bowtie Nanoantenna. *Nat. Photonics* **2009**, *3*, 654–657.
7. Atwater, H. A.; Polman, A. Plasmonics for Improved Photovoltaic Devices. *Nat. Mater.* **2010**, *9*, 205–213.
8. Huang, C.; Bouhelier, A.; Colas des Francs, G.; Bruyant, A.; Guenot, A.; Finot, E.; Weeber, J.-C.; Dereux, A. Gain, Detuning, and Radiation Patterns of Nanoparticle Optical Antennas. *Phys. Rev. B* **2008**, *78*, 155407.
9. Ko, H.; Singamaneni, S.; Tsukruk, V. V. Nanostructured Surfaces and Assemblies as SERS Media. *Small* **2008**, *4*, 1576–1599.
10. Schuck, P. J.; Fromm, D. P.; Sundaramurthy, A.; Kino, G. S.; Moerner, W. E. Improving the Mismatch between Light and Nanoscale Objects with Gold Bowtie Nanoantennas. *Phys. Rev. Lett.* **2005**, *94*, 017402.
11. Wenger, J.; Gérard, D.; Bonod, N.; Popov, E.; Rigneault, H.; Dintinger, J.; Mahboub, O.; Ebbesen, T. W. Emission and Excitation Contributions to Enhanced Single Molecule Fluorescence by Gold Nanometric Apertures. *Opt. Express* **2008**, *16*, 3008–3020.
12. Chen, Y.; Munechika, K.; Jen-La Plante, I.; Munro, A. M.; Skrabalak, S. E.; Xia, Y.; Ginger, D. S. Excitation Enhancement of CdSe Quantum Dots by Single Metal Nanoparticles. *Appl. Phys. Lett.* **2008**, *93*, 053106.
13. Alivisatos, A. P. Semiconductor Clusters, Nanocrystals, and Quantum Dots. *Science* **1996**, *271*, 933–937.
14. Klimov, V. I. Spectral and Dynamical Properties of Multiexcitons in Semiconductor Nanocrystals. *Annu. Rev. Phys. Chem.* **2007**, *58*, 635–673.
15. Fisher, B.; Caruge, J. M.; Zehnder, D.; Bawendi, M. Room-Temperature Ordered Photon Emission from Multiexciton States in Single CdSe Core-Shell Nanocrystals. *Phys. Rev. Lett.* **2005**, *94*, 087403.
16. Bonati, C.; Mohamed, M. B.; Tonti, D.; Zgrablic, G.; Haacke, S.; van Mourik, F.; Chergui, M. Spectral and Dynamical Characterization of Multiexcitons in Colloidal CdSe Semiconductor Quantum Dots. *Phys. Rev. B* **2005**, *71*, 205317.
17. Nair, G.; Bawendi, M. G. Carrier Multiplication Yields of CdSe and CdTe Nanocrystals by Transient Photoluminescence Spectroscopy. *Phys. Rev. B* **2007**, *76*, 081304.
18. Ben-Haim, N. R.; Oron, D. Optical Sectioning by Multiexcitonic Ladder Climbing in Colloidal Quantum Dots. *Opt. Lett.* **2008**, *33*, 2089–2091.
19. Wenger, J.; Rigneault, H. Photonic Methods to Enhance Fluorescence Correlation Spectroscopy and Single Molecule Fluorescence Detection. *Int. J. Mol. Sci.* **2010**, *11*, 206–221.
20. Genet, C.; Ebbesen, T. W. Light in Tiny Holes. *Nature* **2007**, *445*, 39–46.
21. Aouani, H.; Wenger, J.; Gérard, D.; Rigneault, H.; Devaux, E.; Ebbesen, T. W.; Mahdavi, F.; Xu, T.; Blair, S. Crucial Role of the Adhesion Layer on the Plasmonic Fluorescence Enhancement. *ACS Nano* **2009**, *3*, 2043–2048.
22. Fisher, B.; Caruge, J. M.; Chan, Y.-T.; Halpert, J.; Bawendi, M. G. Multiexciton Fluorescence from Semiconductor Nanocrystals. *Chem. Phys.* **2005**, *318*, 71–81.
23. Fisher, B. R.; Eisler, H.-J.; Stott, N. E.; Bawendi, M. G. Emission Intensity Dependence and Single-Exponential Behavior In Single Colloidal Quantum Dot Fluorescence Lifetimes. *J. Phys. Chem. B* **2004**, *108*, 143–148.
24. Gérard, D.; Wenger, J.; Devilez, A.; Gachet, D.; Stout, B.; Bonod, N.; Popov, E.; Rigneault, H. Strong Electromagnetic Confinement near Dielectric Microspheres to Enhance Single-Molecule Fluorescence. *Opt. Express* **2008**, *16*, 15297–15303.
25. Devilez, A.; Bonod, N.; Stout, B.; Gérard, D.; Wenger, J.; Rigneault, H.; Popov, E. Three-Dimensional Subwavelength Confinement of Photonic Nanojets. *Opt. Express* **2009**, *17*, 2089–2094.
26. Gérard, D.; Devilez, A.; Aouani, H.; Stout, B.; Bonod, N.; Wenger, J.; Popov, E.; Rigneault, H. Efficient Excitation and Collection of Single Molecule Fluorescence Close to a Dielectric Microsphere. *J. Opt. Soc. Am. B* **2009**, *26*, 1473–1478.
27. Gérard, D.; Wenger, J.; Bonod, N.; Popov, E.; Rigneault, H.; Mahdavi, F.; Blair, S.; Dintinger, J.; Ebbesen, T. W. Nanoaperture-Enhanced Fluorescence: Towards Higher Detection Rates with Plasmonic Metals. *Phys. Rev. B* **2008**, *77*, 045413.
28. Jiao, X.; Goeckeritz, J.; Blair, S.; Oldham, M. Localization of Near-Field Resonances in Bowtie Antennae: Influence of Adhesion Layers. *Plasmonics* **2009**, *4*, 37–50.
29. Mahdavi, F.; Liu, Y.; Blair, S. Modeling Fluorescence Enhancement from Metallic Nanocavities. *Plasmonics* **2007**, *2*, 129–142.
30. Popov, E.; Neviere, M.; Wenger, J.; Lenne, P.-F.; Rigneault, H.; Chaumet, P.; Bonod, N.; Dintinger, J.; Ebbesen, T. W. Field Enhancement in Single Subwavelength apertures. *J. Opt. Soc. Am. A* **2006**, *23*, 2342–2348.